A System for Automated Detection of Ampoule Injection Impurities

Ji Ge, *Member, IEEE*, Shaorong Xie, Yaonan Wang, Jun Liu, *Student Member, IEEE*, Hui Zhang, Bowen Zhou, Falu Weng, Changhai Ru, *Member, IEEE*, Chao Zhou, Min Tan, and Yu Sun, *Fellow, IEEE*

***Abstract*—Ampoule injection is a routinely used treatment in hospitals due to its rapid effect after intravenous injection. During manufacturing, tiny foreign particles can be present in the ampoule injection. Therefore, strict inspection must be performed before ampoule injections can be sold for hospital use. In the quality control inspection process, most ampoule enterprises still rely on manual inspection which suffers from inherent inconsistency and unreliability. This paper reports an automated system for inspecting foreign particles within ampoule injections. A custom-designed hardware platform is applied for ampoule transportation, particle agitation, and image capturing and analysis. Constructed trajectories of moving objects within liquid are proposed for use to differentiate foreign particles from air bubbles and random noise. To accurately classify foreign particles, multiple features including particle area, mean gray value, geometric invariant moments, and wavelet packet energy spectrum are used in supervised learning to generate feature vectors. The results show that the proposed algorithm is effective in classifying foreign particles and reducing false positive rates. The automated inspection system inspects over 150 ampoule injections per minute (versus ~ 12 ampoule injections per minute by technologist) with higher accuracy and repeatability. In addition, the automated system is capable of diagnosing impurity types while existing inspection systems are not able to classify detected particles.**

***Note to Practitioners*—Present quality assessment of ampoule injections in pharmaceutical manufacturing relies on manual operation by certified technologists or machine-assisted detection systems. Existing technologies are not able to effectively distinguish symbols/dirt on the surface of an ampoule, air bubbles, and random noise from foreign particles inside the ampoule. This paper reports an automated ampoule inspection system consisting of two working stations (high-speed revolving station and abruptly stopping station). The system agitates particles and rotates them spirally along the axis of the ampoule container. Based on image processing and trajectories construction, foreign particles are effectively detected and distinguished from air bubbles and random noise.**

***Index Terms*—Ampoule injection inspection, automated ampoule inspection, foreign particles, impurity detection, supervised learning.**

Manuscript received June 14, 2015; revised August 07, 2015; accepted October 06, 2015. Date of publication November 04, 2015; date of current version April 05, 2017. This paper was recommended for publication by Associate Editor T. Kawahara and Editor J. Wen upon evaluation of the reviewers' comments. The work of Y. Sun was supported by the Canada Research Chairs Program. This work was supported in part by the National Natural Science Foundation of China under Grant 61305019, Grant 61463018, Grant 61401046, and Grant 61528304, and in part by the Natural Science Foundation of Jiangxi Province under Grant 20132BAB211032, Grant 20151BAB207046, and Grant GJJ13385, in part by the Shanghai Municipal Science and Technology Commission Project under Grant 14JC1491500, and in part by the International S&T Cooperation Program of China under Grant 2014DFA70470. *(Corresponding authors: Ji Ge, Shaorong Xie, Yaonan Wang, and Yu Sun.)*

J. Ge is with the Advanced Micro and Nanosystems Laboratory, University of Toronto, Toronto, ON M5S 3G8, Canada, and also with the College of Electrical Engineering and Automation, Jiangxi University of Science and Technology, Ganzhou 341000, China (e-mail: jige@mie.utoronto.ca; geji1981@gmail.com).

S. Xie is with the School of Mechatronic Engineering and Automation, Shanghai University, Shanghai 200072, China (e-mail: srxie@shu.edu.cn).

Y. Wang is with the College of Electrical and Information Engineering, Hunan University, Changsha 410082, China (e-mail: yaonan@hnu.edu.cn).

J. Liu is with the Advanced Micro and Nanosystems Laboratory, University of Toronto, Toronto, ON M5S 3G8, Canada (e-mail: ljun@mie.utoronto.ca).

H. Zhang is with the College of Electrical and Information Engineering, Changsha University of Science and Technology, Changsha 410012, China (e-mail: zhanghuihby@hotmail.com).

B. Zhou is with the Department of Electrical Engineering, Hunan University of Science and Technology, Xiangtan 411201, China (e-mail: bowenzhou@163.com).

F. Weng is with the College of Electrical Engineering and Automation, Jiangxi University of Science and Technology, Ganzhou 341000, China (e-mail: wengfalu@hotmail.com).

C. Ru is with the Research Center of Robotics and Micro System and Collaborative Innovation Center of Suzhou Nano Science and Technology, Soochow University, Suzhou, 215021, China, and also with the College of Automation, Harbin Engineering University, Harbin, 150001, China (e-mail: rzh@suda.edu.cn).

C. Zhou and M. Tan are with Institute of Automation, Chinese Academy of Sciences, Beijing 100190, China (e-mail: chao.zhou@ia.ac.cn; min.tan@ia.ac.cn).

Y. Sun is with the Advanced Micro and Nanosystems Laboratory, University of Toronto, Toronto, ON M5S 3G8, Canada (e-mail: sun@mie.utoronto.ca).

Color versions of one or more of the figures in this paper are available online at http://ieeexplore.ieee.org.

Digital Object Identifier 10.1109/TASE.2015.2490061

I. Introduction

An ampoule, which is commonly made of glass, is a small sealed vial used to contain and preserve liquid injectable pharmaceuticals. Ampoule injection [see Fig. 1(a)] plays an important role in clinical treatment due to its instant effect after intravenous injection. Because of imperfect control in ampoule manufacturing, certain particles such as glass chips, rubber chips, chemical fibers, and hair may appear in the liquid medicine due to the degradation of the filtering system in manufacturing, decreased purification level of the factory, and carbonization during container sealing [1]. These tiny foreign particles (diameters $< 100\ \mu$m) cannot be metabolized by the human body and can cause thrombus, phlebitis, tumor, anaphylactic reaction or even death when they are injected into the human vein [2], [3]. Presence of these particles has been one of the top ten reasons for the recalls of liquid pharmaceuticals [4].

Although the probability of particle presence is low ($< 0.35\%$), manufactured injections require 100% strict inspection prior to entering the market, according to the regulations

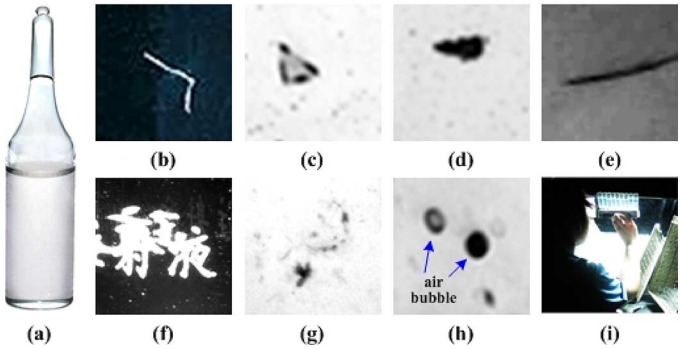

Fig. 1. Sample images of typical foreign particles and disturbances. (a) Ampoule injection. (b) Fiber. It usually comes from clothes or filtering system. (c), (d) Glass chips. They usually come from incomplete container cleaning or sealing. (e) Hair. (f), (g) Label and dirt on surface of the ampoule. (h) Air bubbles in the liquid. (i) Manual inspection.

of U.S. Food and Drug Administration (FDA) [5]. Fig. 1 shows typical insoluble foreign particles and disturbances (e.g., labeling or dirt on the ampoule surface, air bubbles inside ampoule). Presently, more than 95% pharmaceutical manufacturers in developing countries still adopt manual inspection for quality control [6]. In manual inspection [see Fig. 1(i)], an inspector rotates and flips over the injection container gently under fluorescent lighting in a darkroom. Rotating and flipping makes foreign particles suspended or move in liquid medicine. The inspector based on experience determines whether the product is acceptable. "Light blocking" is also used in laboratories for detecting and sizing particles larger than 1 μm, based on the amount of light a particle blocks when passing through the detection area [7]. Light attenuation, flicker or bubbles existing in the injection can lead to high false positive or false negative inspection rates. Subjective judgement, low efficiency, and human fatigue call for automated inspection.

Most pharmaceutical manufacturers in developed countries rely on machine-assisted inspection [8]. Semi-automated machines (e.g., Dabrico DI-100 LT/XL) automate the agitation of ampoules one at a time by mimicking human operators. The machine is also equipped with convex lens that magnify particles for human operator to observe. Air bubbles generated during ampoule agitation can distract the inspector and cause high false positive rates. In addition, the serial inspection process is slow and easily causes human fatigue. The "light blocking" method [9] is adopted by Japan Eisai in their automated inspection machine AIM288. A halogen bulb is used as the light source, and a sensor is used to identify slight variations of light absorbance when particles pass the detection area. For CCD/CMOS camera-based automated inspection machines (e.g., Seidenader XS), sequential images of an ampoule injection are captured, and frame differencing is applied to detect foreign targets. Unfortunately, false positive rates become high for both the light blocking and CCD/CMOS-based automated inspection machines when air bubbles or random noise are present during ampoule agitation. Furthermore, existing automated inspection machines are not able to classify the detected foreign particles although classification is desired by the pharmaceutical manufacturing industry.

To automate the inspection process and achieve proper classification of foreign particles, a number of challenges must be tackled. Several types of foreign particles can be present in the ampoule injection. No prior knowledge such as the exact size or position of the foreign particles can be used for particle feature extraction or trajectory tracking. Hence, traditional particle size or shape-based object detection algorithms cannot be applied. After detection, they need to be properly differentiated from air bubbles and scratches or marks on the ampoule surface. Particles in an ampoule need to be stirred up for recognition through their moving trajectories. In human operation or existing machine-assisted inspection machines, an ampoule is flipped over to agitate foreign particles. However, this agitation approach often undesirably generates air bubbles. "Linear chain/belt conveyor" and "rotary platform" are the two main designs for container transportation in production lines [10]. On a linear conveyor, containers are moved in a straight line. However, this approach typically requires larger space than rotary platforms where containers are transported among several star wheels and cameras are installed around them. Therefore, a rotary platform was developed in our work.

Algorithms such as 3D matched filtering [11], [12], multistage hypothesis testing [13], dynamic programming [14], [15], and Markov random field-based contour tracking [16] have been reported for detecting weak, moving targets immersed in a noisy background. These algorithms detect low-contrast objects by accumulating their trajectory energies based on the moving disciplines of the particles between frames. Typically, multiple threshold values need to be determined for these algorithms to properly track moving objects. These algorithms are also computationally costly and require significant storage space for storing intermediate results. Other algorithms that can be used to detect foreign particles in liquid are the support vector machine (SVM) [17], [18], sub-pixel registration and frame differencing [19], and probability weighted threshold and Kalman filter [20]. Compared to these methods, the online sequential extreme learning machine (OS-ELM) [21], [22] with spatial information used in the present work is more effective in distinguishing particles from air bubbles or random noise. Due to variations in foreign particle size and color across ampoule injections, it is unreliable to rely solely on calculating the target's mean pixel intensity value. Hence, in the supervised learning method used in our system, feature vector is constructed with multiple cues including foreign particle size, mean gray value, gray variance, geometric invariant moments, and wavelet packet energy spectrum.

II. System Design

A. Hardware Platform

Two stations, a high-speed rotating station (HSRS) and an abruptly stopping station (ASS), form the rotary platform-based inspection line, as shown in Fig. 2(a). An active spring-loaded clamping mechanism [Fig. 2(c)] is designed to stir up foreign particles from the bottom of the ampoule container. With the HSRS and ASS stations, automated ampoule movements (i.e., steady clamping, high-speed rotation, and abrupt stop) are realized, and smooth moving trajectories of foreign particles are achieved to facilitate detection.

In the HSRS station, the rotating tray is driven by a motor located underneath the machine table. It rotates at a speed of 1500 rpm as the injection container triggers a photoelectric

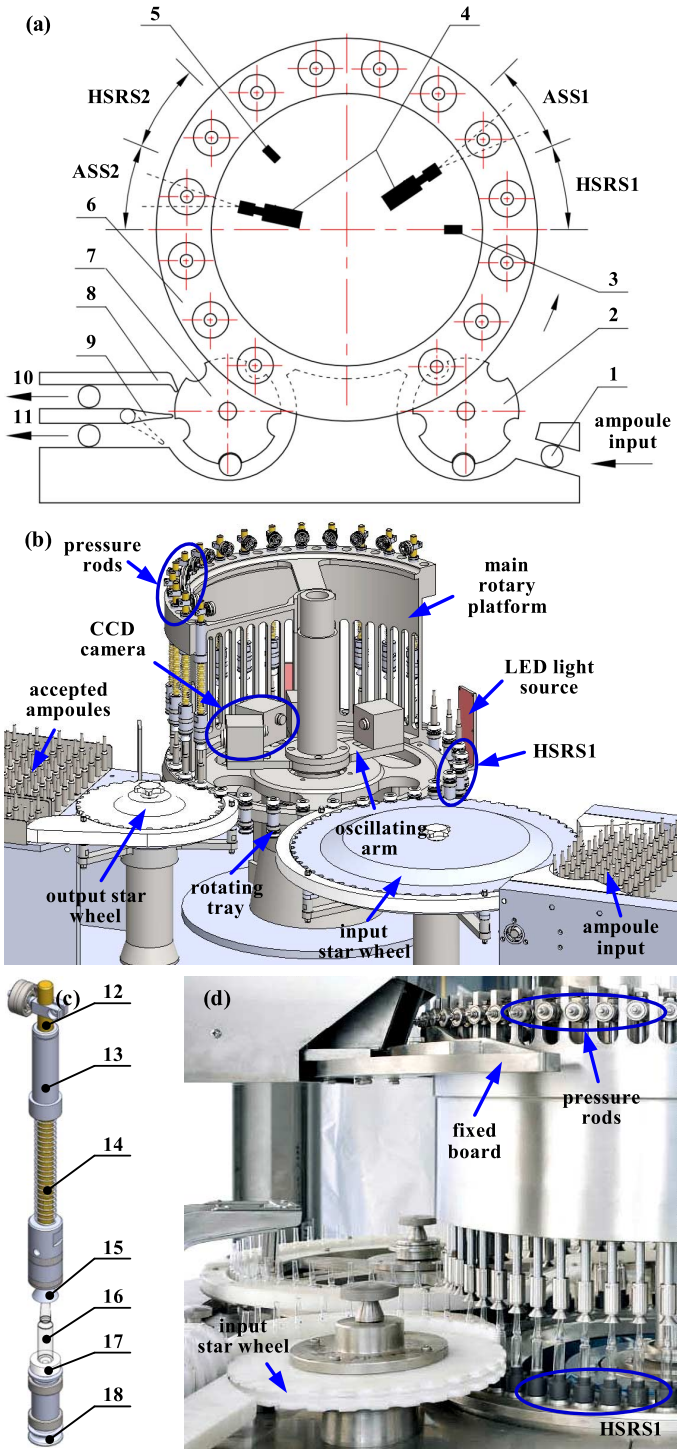

Fig. 2. (a) Top view of the automated ampoule inspection system (1. ampoule injection; 2. input star wheel; 3. photoelectric sensor I; 4. CCD camera; 5. photoelectric sensor II; 6. main rotary platform; 7. output star wheel; 8. baffle; 9. striking fork; 10. rejected products output; 11. qualified products output). (b) Section view of the automated ampoule inspection machine. (c) Active spring-loaded clamping mechanism (12. pressure rod; 13. flanged sleeve; 14. spring; 15. rotatable cap; 16. ampoule injection; 17. rotating tray; 18. V-belt pulley). (d) A snapshot of the constructed system.

sensor. The main rotary platform and input and output star wheels rotate synchronously through connecting their respective gears located underneath the machine table, and they are driven by only one 1.1 kW single-phase induction motor (YCJ90L2, Regal Beloit Company). The rotating tray and the pressure rods ensure containers' steady rotation and reduce the occurrence probability of air bubbles. Ampoules are stopped abruptly as they enter the ASS station, and the generated vortex lifts particles off from the bottom of the ampoule container. In the meanwhile, CCD cameras are triggered to capture ten sequential images for foreign particle detection.

As shown in Fig. 2(b), the vision system consists of three LED light sources (two array-type backlight LED, Schott Moritex Co., emitting surface dimension: 20 mm × 80 mm, and one bottom LED light source with two fiber heads, PFB2-20SW-F, CCS Inc., Japan), and four CCD cameras (MVC685DAM-GE110, Microview; frame rate: 110 fps). In each of the two ASS stations, two CCD cameras are arranged to inspect two ampoules labeled with odd and even number, respectively. Back and bottom light illuminations of the ampoule injection are applied in each ASS station. The "ampoule tracing" is realized by the oscillating arm. Object distance of the camera was set to be 95 mm. The system takes 0.8 s to complete the inspection of one ampoule, including ampoule transportation, image capturing and processing, and ampoule sorting.

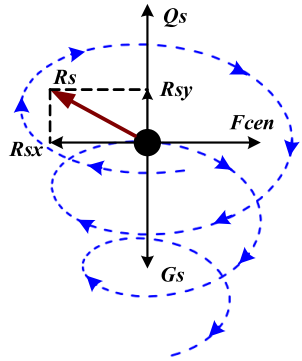

Fig. 3. Force analysis of when a particle moves in liquid. G_s, Q_s, R_s, and F_{cen} denote gravity, buoyancy, viscous force and centrifugal force of the particle, respectively.

B. Kinetics of Moving Particles in Liquid

After rotation and abrupt stopping of the ampoule containers, ten sequential images were captured to record the trajectory of particles. Throughout this process, Reynolds number (Re) for every ampoule injection always satisfies $Re > 4,000$ (i.e., turbulent flow and vortices are produced). Foreign particles within liquid experience several forces, as illustrated in Fig. 3. The dash line indicates the moving trajectory of the particle. In the vertical direction, forces include gravity G_s, buoyancy Q_s, and the vertical component of viscous force R_{sy}. In the horizontal direction, there are centrifugal force F_{cen} and horizontal component of viscous force R_{sx}. Hence, net forces in the vertical direction F_{vnet} and the horizontal direction F_{hnet} are

$$\begin{aligned} F_{vnet} &= G_s - Q_s - R_{sy} \\ &= \frac{\pi}{18} \cdot \rho_l \cdot {d_s}^2 \cdot {v_y}^2 + \frac{\pi}{6} \cdot d_s^3 \cdot g \cdot (\rho_s - \rho_l) \end{aligned} \tag{1}$$

$$F_{hnet} = F_{cen} - R_{sx} = \frac{\pi}{6} \cdot {d_s}^3 \cdot \rho_s \cdot r \cdot w^2 + \frac{\pi}{18} \cdot \rho_l \cdot {d_s}^2 \cdot {v_x}^2 \tag{2}$$

where ρ_l is liquid density; ρ_s is particle density; d_s is diameter of the foreign particle; v_x and v_y are horizontal and vertical components of particle's linear moving velocity; r and w are rotating radius and angular velocity of the particle. According to Newton's second law, (1) can be rewritten as

$$\frac{dv_y}{dt} = \frac{\rho_l}{3 \cdot d_s \cdot \rho_s} \cdot {v_y}^2 + g \cdot \left(1 - \frac{\rho_l}{\rho_s}\right). \tag{3}$$

Assume the initial condition to be $\{v_y | t = 0\} = V_0$, then v_y is

$$v_y = -M^{-1} \cdot \tan(N \cdot t + \arctan(M \cdot V_0)) \tag{4}$$

where $M = [\rho_l/(3 \cdot d_s \cdot g \cdot (\rho_s - \rho_l))]^{1/2}$, and $N = \left[(\rho_l \cdot g \cdot (\rho_s - \rho_l))/(3 \cdot d_s \cdot {\rho_s}^2)\right]^{1/2}$. Denote the camera's frame rate by f, then the moving distance in the vertical direction between the first and nth frames is

$$y_n = -M^{-1} \cdot \tan\left(\frac{N \cdot n}{f} + \arctan(M \cdot V_0)\right). \tag{5}$$

These sequential values $\{y_1, y_2, \ldots, y_n\}$ and smooth trajectories significantly facilitate the differentiation of foreign particles from air bubbles or other disturbances.

III. Particle Recognition

Among machine learning methods, SVMs are only directly applicable for two-class tasks, making it unsuitable for particle classification in ampoule inspection. The classification accuracy of SVMs highly depends on kernel selection, kernel's parameters, and soft margin parameter. In comparison, online sequential extreme learning machine (OS-ELM) [21] is faster by orders of magnitude in learning and prediction than SVMs [23], [24] and back-propagation algorithms [25], [26]. Furthermore, parameters (e.g., learning rate or stopping criteria) of OS-ELM do not require manual tuning. For the purpose of distinguishing particles from air bubbles using OS-ELM, this work proves that spatial information (i.e., coordinates of object centroid) must be applied to construct a target's moving trajectory. The trajectory of a moving particle is continuous and downward while an air bubble's trajectory is continuous and upward. This spatial-based OS-ELM approach is experimentally proven in this work to be effective in foreign particle classification, especially for accurate differentiation of air bubbles from glass chips. Fig. 4 shows the flowchart for the recognition of foreign particles. Key steps are highlighted in blue and discussed in the following sections.

A. Feature Extraction

Features of tiny foreign particles in ampoule injection include area, shape, mean gray value, and statistical properties. Extracted features should ideally have significant differences among classes and have little change in translation and rotation for the same target in sequential images. Therefore, besides particle area, mean gray value and gray variance, features including Hu's invariant moments, Zernike moment Z_{20}, ratio L/W between length L and width W of the minimum bounding rectangle, and occupation ratio of the particle A/LW are also included in the feature vectors.

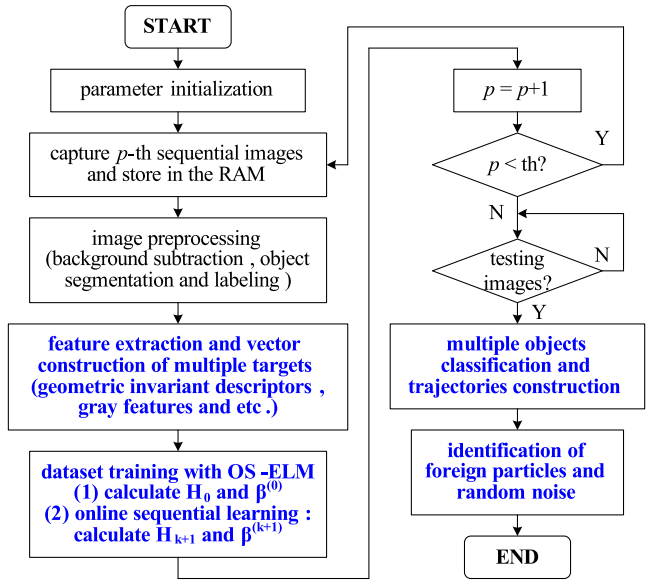

Fig. 4. Flowchart of foreign particle detection and classification using the spatial OS-ELM method.

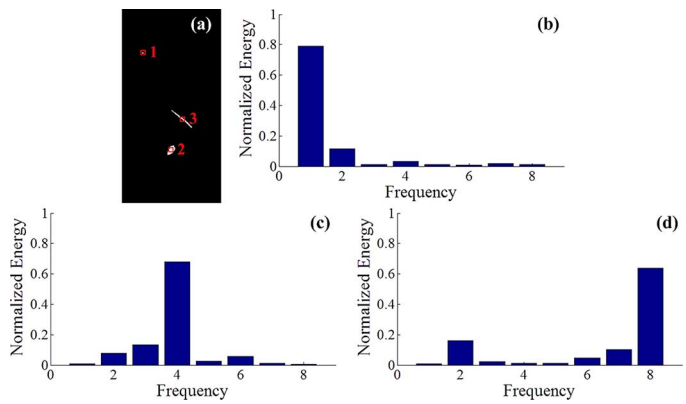

Fig. 5. Normalized wavelet packet energy spectrum. (a) Difference image with fiber, glass chip, and random noise which are labeled with red rectangular. (b), (c) and (d) Show the wavelet packet energy spectrum of glass chip, fiber and random noise, respectively.

From the perspective of energy, the various kinds of foreign particles in ampoule have different energy distributions. One-dimensional signal is constructed through accumulating target's pixel gray values vertically. Energy distribution is then depicted through calculating the wavelet packet energy spectrum of this signal. Fig. 5 shows an example of energy distribution variations among glass chip, fiber, and random noise. It was found that five decomposition levels of the wavelet packet are sufficiently accurate to interpret fine details of the signal. Principal component analysis [27] is applied to reduce the dimension of calculated wavelet packet energy spectrum. In Fig. 5, normalized maximal energy appearing at first, fourth, and eighth principal component denotes glass chip, fiber and random noise, respectively. Hence, four principal components of object's wavelet packet energy spectrum $E_{51} \sim E_{54}$ are also included in the feature vector which dimension reaches 17, where subscript "5" is the decomposition level of the wavelet packet.

B. Classification and Trajectory Construction

Assume the number of images is I, the number of objects in each image is J, the number of extracted features of each object is K. Hence, the feature vector can be generalized as

$$P_{uvw} = \{p_{uvw} | u \in [1, I], v \in [1, J], w \in [1, K]\} \quad (6)$$

where u, v, w denote the ordinal number of frame, object, and feature, respectively. If the number of object in the uth image is v, extracted feature vector can be written as

$$\begin{aligned} P_{u1} &= \{p_{u11}, p_{u12}, \ldots, p_{u1K}\}, \\ P_{u2} &= \{p_{u21}, p_{u22}, \ldots, p_{u2K}\}, \ldots, \\ P_{uv} &= \{p_{uv1}, p_{uv2}, \ldots, p_{uvK}\}. \end{aligned}$$

Its matrix format is

$$P_{IJ} = \begin{bmatrix} P_{11} & P_{12} & \cdots & P_{1J} \\ P_{21} & P_{22} & \cdots & P_{2J} \\ \cdots & \cdots & \cdots & \cdots \\ P_{I1} & P_{I2} & \cdots & P_{IJ} \end{bmatrix}. \quad (7)$$

Connecting the elements of $(I \times J)$-dimensional matrix P_{IJ} row by row and differentiating them from each other with OS-ELM, $(IJ \times 1)$-dimensional column vector is

$$P_{IJ} = (P_{11}, \ldots, P_{1J}, P_{21}, \ldots, P_{2J}, \ldots, P_{I1}, \ldots, P_{IJ})^T. \quad (8)$$

Those objects grouped into one class are considered the same target. For instance, if P_{13}, P_{22}, P_{35}, P_{43}, and P_{52} are grouped into one class, then the third object in frame 1, second object in frame 2, fifth object in frame 3, third object in frame 4, and second object in frame 5 are considered the same target. The moving trajectory of the object is constructed by connecting these centroids of the same target across sequential images.

IV. Experimental Results and Discussion

A. Training Dataset Construction

In experiments, 1000 ampoules containing typical foreign particles (e.g., glass chips, rubber chips, fiber, and hair), were selected by certified technologists. The system captured five sequential images of each ampoule after ampoule rotation and abrupt stopping. Hence, a (5000×18)-dimensional matrix was constructed with 17 foreign particle features and 1 type index (TI). Here, TI has values of 1, 2, 3 or 4, denoting glass chips, rubber chips, fiber, and hair, respectively

$$\begin{aligned} \text{Feature} &= (HU, Z_{20}, A, G, Q, E, GV, V, TI) \\ &= \begin{bmatrix} hu_1 & z_1 & a_1 & g_1 & q_1 & e_1 & gv_1 & v_1 & t_1 \\ hu_2 & z_2 & a_2 & g_2 & q_2 & e_2 & gv_2 & v_2 & t_2 \\ \vdots & \vdots & \vdots & \vdots & \vdots & \vdots & \vdots & \vdots & \vdots \\ hu_k & z_k & a_k & g_k & q_k & e_k & gv_k & v_k & t_k \end{bmatrix} \end{aligned} \quad (9)$$

where $k = 5,000$; HU are Hu's seven invariant moments $h_1, h_2, \ldots, h_7$; Z_{20} is the Zernike moment; A, G and Q are area, L/W, and A/LW; E is the wavelet packet energy spectrum; GV, V and TI denote the mean gray value, variance and type index of the foreign particles.

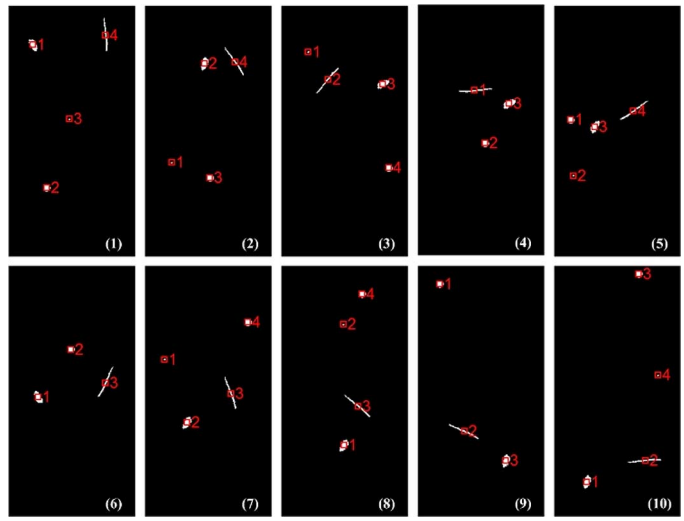

Fig. 6. Ten sequential ampoule images; all targets are extracted and labeled with red squares after image preprocessing. Labeled numbers in every image are determined by abscissa of the target.

B. Trajectory-Based Particle Recognition

Ten captured sequential images of an ampoule injection, containing fiber and glass chip, were randomly selected as an example to evaluate recognition accuracy. Besides foreign particles, air bubble and random noise also appeared in these selected sequential images. As shown in Fig. 6, each target was extracted and labeled with a red square after image preprocessing (i.e., background subtraction, object segmentation, and labeling). Labeled numbers in every image are determined according to abscissa of the target.

In these ten images, a (37×17)-dimensional feature matrix generated by 37 targets were normalized and classified by OS-ELM. The number of normalized datasets was determined by the maximum number of objects in every image. In this example, four groups should be achieved (i.e., objects "P_{11}, P_{22}, P_{33}, P_{43}, P_{53}, P_{61}, P_{72}, P_{81}, P_{93}, P_{101}," "P_{12}, P_{23}, P_{34}, P_{42}, P_{51}, P_{62}, P_{74}, P_{84}, P_{91}, P_{103}," "P_{13}, P_{21}, P_{31}, P_{52}, P_{71}, P_{82}, P_{104}," and "P_{14}, P_{24}, P_{32}, P_{41}, P_{54}, P_{63}, P_{73}, P_{83}, P_{92}, P_{102}") and classified into glass chip, air bubble, random noise, and fiber, respectively. As illustrated in Fig. 7, moving trajectories of the objects within each group were constructed by connecting their coordinates frame by frame.

As shown in Fig. 7(a) and (b), experimental trajectory of foreign particle with larger density (e.g., fiber and glass chips) is downward while air bubble's trajectory is upward, which is consistent with estimates from (5). It can also be observed that rotation radius of the target becomes smaller with particles falling down or air bubbles floating up due to liquid viscosity. In the model described in Section II-B, particle's shape is assumed to be spherical. This simplification was made for modeling feasibility since different types of impurities (e.g., glass chips, rubber chips, and fibers) have varied shapes. Although different shapes can lead to modeling differences, the simplified model with the spherical shape assumption was experimentally proven effective for predicting particle trajectories, as shown in Fig. 7(a) and (b). In Fig. 7(c), random noise disappeared in some images (see frames 4, 6, and 9) and its trajectory displays random fluctuations. Therefore, foreign particles in ampoule

TABLE I
COMPARISONS OF LIBSVM, ELM, AND SPATIAL OS-ELM (CPU: INTEL CORE I5, RAM: 4 GB, WINDOWS 7 PROFESSIONAL, MATLAB 2013A)

algorithm	training mode	#nodes	activation function	time (msec)		classification accuracy (%)	
				training	testing	training	testing
LIBSVM	/	/	/	262.93	82.70	97.22	93.49
ELM	batch	25	Sigmoid	15.50	**3.17**	97.01	92.80
		25	Sine	**15.28**	3.88	96.94	92.73
		25	Hardlim	16.01	4.15	97.11	93.55
Spatial OS-ELM	1-by-1	25	Sigmoid	121.97	12.18	96.74	92.58
		25	Sine	110.85	11.51	97.17	**94.14**
		25	Hardlim	183.26	17.24	97.09	93.24
	20-by-20	25	Sigmoid	64.70	6.16	97.18	93.48
		25	Sine	59.12	5.47	97.10	92.81
		25	Hardlim	82.81	7.88	**97.54**	93.77

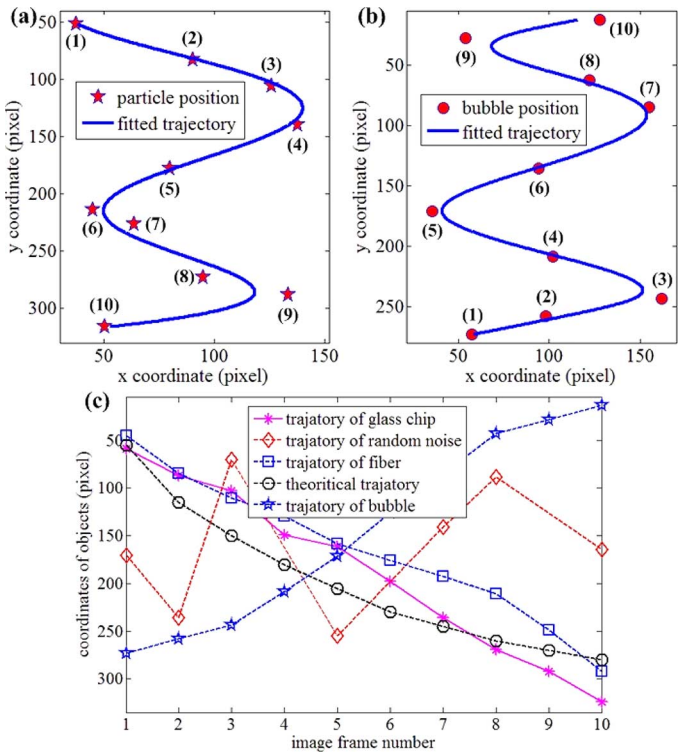

Fig. 7. (a) and (b) Experimental trajectories of glass chip and air bubble. Serial number (1)~(10) represent the image frame number. (c) Trajectories of glass chip, random noise, fiber and air bubble, constructed through connecting their coordinates frame by frame.

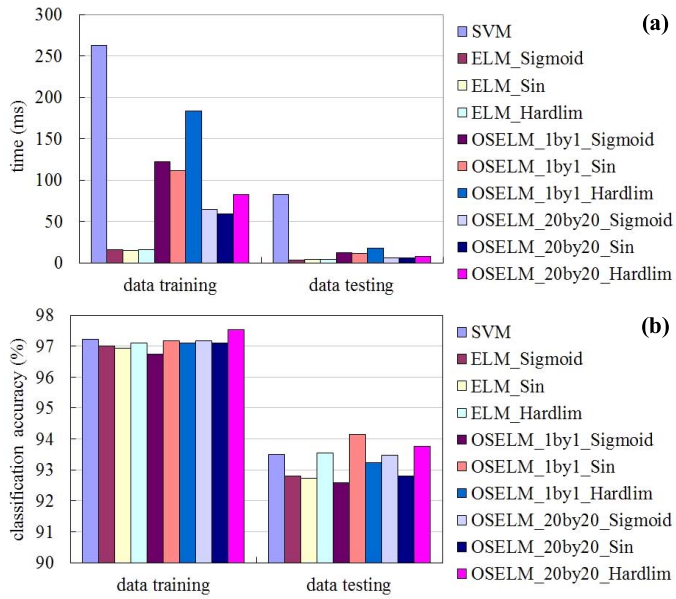

Fig. 8. (a) Comparison of time taken by data training and data testing. (b) Classification accuracy of data training and data testing.

injection can be differentiated from air bubbles and random noise according to their distinct moving trajectory trends.

Particles with large density (versus air bubbles and random noise) are classified using the proposed spatial OS-ELM algorithm. Comparisons of spatial OS-ELM, SVM, and ELM algorithms are summarized in Table I in terms of training, testing time and classification accuracy. The (5000×18)-dimensional feature vector, discussed in Section IV-A, was used as the same training dataset, and a (1500×17)-dimensional matrix generated from additionally captured ampoule images was used as the testing dataset.

As shown in Table I and Fig. 8(a), the LIBSVM algorithm costs more time in both training and testing than the ELM and spatial OS-ELM approaches. Among the three algorithms, the ELM method is the most computationally efficient. For instance, LIBSVM costs more than 250 ms to train the datasets and almost 20 times longer than the ELM method. For the ELM and OS-ELM methods, sequential operation of 1-by-1 takes the longest time followed by 20-by-20 and then the batch mode. Time variations are small for ELM and OS-ELM with different activation functions. Results summarized in Fig. 8(b) show that classification accuracies of training and testing for ELM and OS-ELM with different activation functions are similar. OS-ELM with 1-by-1 training mode produced the highest classification accuracy (94.14%) for all types of foreign particles.

We further quantified classification accuracies with and without considering trajectory trends of particles in spatial OS-ELM. In our experiments, for determining classification accuracies, all the foreign particles identified by the tested

TABLE II
CLASSIFICATION ACCURACIES FOR DIFFERENT TYPES OF FOREIGN PARTICLES AND AIR BUBBLES ("WITH" AND "WITHOUT" REFER TO WHETHER PARTICLE TRAJECTORIES ARE TAKEN INTO ACCOUNT)

classified	glass chip		rubber		hair		fiber		air bubble	
	with	without	with	without	with	without	with	without	with	without
glass chip	**95.82%**	**87.24%**	1.08%	1.67%	0.14%	0.15%	0.11%	0.12%	0	9.43%
rubber	2.14%	2.53%	**97.91%**	**96.47%**	1.22%	1.25%	0.21%	0.24%	0	2.57%
hair	0.85%	0.87%	0.53%	1.06%	**96.37%**	**96.22%**	2.72%	2.81%	0	0.01%
fiber	1.19%	2.34%	0.48%	0.72%	2.27%	2.37%	**96.95%**	**96.81%**	0.01%	0.02%
air bubble	0	7.02%	0	0.08%	0	0.01%	0.01%	0.02%	**99.83%**	**87.97%**

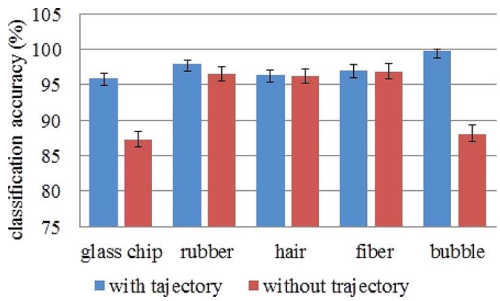

Fig. 9. Classification accuracies between with and without considering trajectory trends of particles.

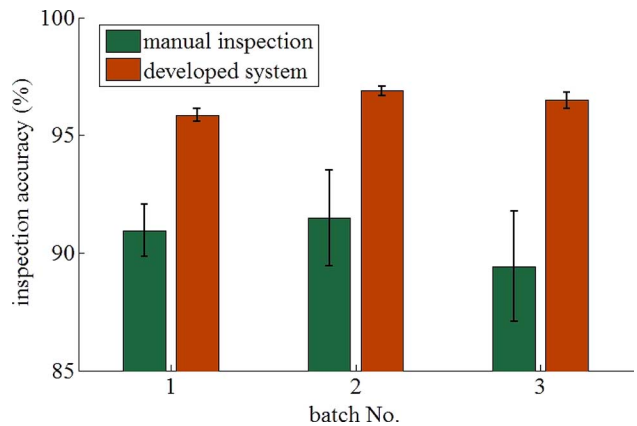

Fig. 10. Inspection accuracy comparison between manual method and the automated system.

algorithms were confirmed by a skilled certified technologist. As summarized in Table II and Fig. 9, the classification accuracy for glass chips is dramatically improved from 87.24% to 95.82% when particle trajectory trend is taken into account. This improvement was achieved because air bubbles were effectively distinguished from glass chips. Classification accuracies for rubber chips, hair, and fiber are all higher than 96%. Air bubbles were identified with 99.83% accuracy when their trajectory trends were considered. Due to slight overlap in appearances and trajectory trends, 2.72% of fibers were mistakenly classified to be hair, and 2.27% of hair were misclassified as fiber.

C. Knapp Test

The "Knapp Test", designed by the U.S. FDA and European Pharmacopoeia, is for evaluating the performance of an inspection system [28]–[30]. In this work, the Knapp Test was conducted using a test set with 170 randomly selected uninspected injections and 80 injections containing particles from the same production batch. These 250 injections were mixed randomly and labeled from 1 to 250. Each injection was first inspected independently ten times by each of the five certified technologists who participated in this study, and then was inspected by the automated inspection system ten times. Two quality factors, QFM_i and QFS_i by manual inspection and automated inspection of each injection were calculated, where $i \in [1, 250]$. Take the 20th injection as an example. If five technologists' rejection times are 8, 6, 8, 8 and 9, the total number of rejection n_{20} is 39. Quality factors of manual inspection QFM_{20} is determined to be $n_{20} \times 10/N = 7.8$, where N is the total number of inspection (i.e., 50 in this example). The quality factor of manual inspection is $QFM = \sum_{i=1}^{250} QFM_i$. According to the "Knapp Test" protocol, only $QFM_i \in (7, 10)$ are added. QFS is calculated using the same procedure.

Maximal value of QFM or QFS is [800, 2500]. The larger for the quality factor, the more accurate the inspection method. If the ratio (i.e., QFS/QFM) is equal or greater than 1, it means that the automated inspection system is equivalent or better than the manual inspection method [29], [30]. In our test, quality factors of the inspection system and manual method were 917 and 796, respectively. The ratio of 1.15 proves that the automated inspection system is superior to manual inspection in detection accuracy.

To more quantitatively compare the inspection accuracy between the manual method and our automated system, three batches of 2 ml-ampoule injections were further tested. In each batch, 400 ampoule injections containing glass chips, rubber chips, fiber, and hair (100 ampoules with each type of particle) were randomly selected and mixed with 400 qualified injections. Every injection was labeled, then evaluated and confirmed by the commercial particle counter (e.g., Puluody PLD-0203, UK). Each batch was inspected by five technologists independently and by our developed system for five times. Inspection accuracy is defined as

$$\text{Accuracy} = \frac{TP + TN}{TP + TN + FP + FN} \tag{10}$$

where TP is the number of true positives, TN is the number of true negatives, FP is the number of false positives, and FN is the number of false negatives.

Data are graphically shown in Fig. 10. The average inspection accuracy was higher than 95.5% for the automated system (versus approximately 90% for the manual method). In addition, the standard deviation of automated counting system was significantly lower than that of manual inspection, which indicates higher precision or repeatability achieved by the automated inspection system. Scrutinizing the false detected situations revealed that they stemmed from lighting disturbances, attenuation of LED light, and shape variations of foreign particles. For instance, in a few cases, the reflection plane of glass chips did not face the CCD camera directly which made the intensity and contrast of the target significantly lower. Therefore, the glass chip could disappear for a period, resulting in a broken trajectory. During fast rotation in the liquid, shape variations of slim fibers could confuse the classifier and lead to a wrongly constructed trajectory of the particle. Present work involves the use of a higher number of sequential images and the development of algorithms for tracking motion-distorted objects, aiming to further reduce the false detection rate.

V. Conclusion

This paper presented an automated system for detecting and classifying foreign particles in ampoule injections. Ampoules were passed through the high-speed rotating station (HSRS) and moved into the abruptly stopping station (ASS) of the inspection system. Ten sequential images for each ampoule injection were captured. Spatial information (i.e., coordinates of the target's centroid) was applied to construct target's moving trajectory which was used as a foreign particle judging criterion. Multiple features of a target including area, mean gray value, geometric invariant moments and wavelet packet energy spectrum were used in supervised learning for predicting/classifying the type of foreign particles. The spatial OS-ELM algorithm was proposed and experimentally proven effective in foreign particle classification. This approach was highly accurate in distinguishing air bubbles from glass chips. Experimental results demonstrated that the automated inspection system achieved high accuracy and repeatability in foreign particle detection and classification.

Acknowledgment

The authors thank Hunan CHINASUN Pharmaceutical Machinery Company, Ltd., Hunan, China, for ampoule injections preparation and manual ampoule inspection by their certified technologists.

References

[1] S. E. Langille, "Particulate matter in injectable drug products," *PDA J. Pharm. Sci. Technol.*, vol. 67, no. 3, pp. 186–200, 2013.

[2] J. H. Bowen, B. H. Woodard, T. K. Barton, P. Ingram, and J. D. Shelburne, "Infantile pulmonary hypertension associated with foreign body vasculitis," *Am. J. Clin. Pathol.*, vol. 75, no. 4, pp. 609–14, Apr. 1981.

[3] P. A. Dewan, H. Ehall, G. A. Edwards, D. J. Middleton, and J. Terlet, "Plastic particle migration during intravenous infusion assisted by a peristaltic finger pump in an animal model," *Pediatr. Surg. Int.*, vol. 18, no. 5–6, pp. 310–4, Sep. 2002.

[4] L. Doessegger, H. C. Mahler, P. Szczesny, H. Rockstroh, G. Kallmeyer, A. Langenkamp, J. Herrmann, and J. Famulare, "The potential clinical relevance of visible particles in parenteral drugs," *J. Pharm. Sci.*, vol. 101, no. 8, pp. 2635–2644, 2012.

[5] M. J. Allport-Settle, *Federal Food, Drug, and Cosmetic Act: The United States Federal FD&C Act Concise Reference*. Middle Creek, NC, USA: PharmaLogika, 2010.

[6] J. Ni, "Production status of mass transfusion and exploration of developing tragedy in China," *China Pharm.*, vol. 13, no. 1, pp. 28–29, 2004.

[7] T. Xu, Y. Gao, and X. Wu, "Analysis of light-blockage principle in small particle size measurement," *Chinese J. Sci. Instrum.*, vol. 26, no. 1, pp. 13–16, 2005.

[8] Y. Wang, J. Ge, H. Zhang, and B. Zhou, "Intelligent injection liquid particle inspection machine based on two-dimensional Tsallis entropy with modified pulse-coupled neural networks," *Eng. Appl. Artif. Intell.*, vol. 24, no. 4, pp. 625–637, Jun. 2011.

[9] Y. C. Agrawal and H. C. Pottsmith, "Instruments for particle size and settling velocity observations in sediment transport," *Mar. Geol.*, vol. 168, no. 1–4, pp. 89–114, 2000.

[10] D. J. Fonseca, G. Uppal, and T. J. Greene, "A knowledge-based system for conveyor equipment selection," *Expert Syst. Appl.*, vol. 26, no. 4, pp. 615–623, 2004.

[11] I. Reed, R. Gagliardi, and H. Shao, "Application of three-dimensional filtering to moving target detection," *IEEE Trans. Aerosp. Electron. Syst.*, vol. AES-19, no. 6, pp. 898–905, Nov. 1983.

[12] M. Xing, Q. Wang, G. Wang, and Z. Bao, "A matched-filter-bank-based 3-D imaging algorithm for rapidly spinning targets," *IEEE Trans. Geosci. Remote Sens.*, vol. 47, no. 7, pp. 2106–2113, Jul. 2009.

[13] S. Blostein and T. Huang, "Detecting small, moving objects in image sequences using sequential hypothesis testing," *IEEE Trans. Signal Process.*, vol. 39, no. 7, pp. 1611–1629, Jul. 1991.

[14] S. Huibo, G. Meiguo, T. Liyu, M. Erke, and G. Wenbin, "An algorithm based on dynamic programming for radar dim multi-target detection," *ACTA Electron. Sin.*, vol. 34, no. 12, pp. 2142–2145, 2006.

[15] W. Yi, L. Kong, J. Yang, and M. R. Morelande, "Student highlight: Dynamic programming-based track-before-detect approach to multi-target tracking," *IEEE Aerosp. Electron. Syst. Mag.*, vol. 27, no. 12, pp. 31–33, Dec. 2012.

[16] C. Chung and H. Chen, "Video object extraction via MRF-based contour tracking," *IEEE Trans. Circuits Syst. Video Technol.*, vol. 20, no. 1, pp. 149–155, Jan. 2010.

[17] Y. Wang, B. Zhou, H. Zhang, and J. Ge, "A vision-based intelligent inspector for wine production," *Int. J. Mach. Learn. Cybern.*, vol. 3, no. 3, pp. 193–203, Sep. 2012.

[18] J. Wen and B. Wang, "Recognition of floating particles in ampoules by wavelet packet energy spectrum and SVM," *Opt. Precis. Eng.*, vol. 17, no. 11, pp. 2794–2799, 2009.

[19] Y. Qin and B. Wang, "Study of on-line inspection technique for foreign substance in Ampoule," in *Proc. 2nd Int. Conf. Artif. Intell. Manag. Sci. Electron. Commer.*, Aug. 2011, pp. 4342–4345.

[20] S. Yang and Y. Wang, "On line detection and tracking method of foreign substances in ampoules in high-speed pharmaceutical lines," *Chinese J. Sci. Instrum.*, vol. 32, no. 3, pp. 488–494, 2011.

[21] N.-Y. Liang, G.-B. Huang, P. Saratchandran, and N. Sundararajan, "A fast and accurate online sequential learning algorithm for feedforward networks," *IEEE Trans. Neural Netw.*, vol. 17, no. 6, pp. 1411–1423, Nov. 2006.

[22] G.-B. Huang, Q.-Y. Zhu, and C.-K. Siew, "Extreme learning machine: Theory and applications," *Neurocomputing*, vol. 70, pp. 489–501, 2006.

[23] C. W. Hsu and C. J. Lin, "A comparison of methods for multiclass support vector machines," *IEEE Trans. Neural Networks*, vol. 13, no. 2, pp. 415–425, Mar. 2002.

[24] C. J. C. Burges, "A tutorial on support vector machines for pattern recognition," *Data Min. Knowl. Discov.*, vol. 2, no. 2, pp. 121–167, 1998.

[25] Y. Yu, T. M. Choi, and C. L. Hui, "An intelligent quick prediction algorithm with applications in industrial control and loading problems," *IEEE Trans. Autom. Sci. Eng.*, vol. 9, no. 2, pp. 276–287, Apr. 2012.

[26] H. K. H. Kim, K. L. K. Lee, B. J. B. Jeon, and C. S. C. Song, "Quick wafer alignment using feedforward neural networks," *IEEE Trans. Autom. Sci. Eng.*, vol. 7, no. 2, Apr. 2010.

[27] M. Ringnér, "What is principal component analysis?," *Nat. Biotechnol.*, vol. 26, no. 3, pp. 303–4, Mar. 2008.

[28] J. A. Melchore, "Sound practices for consistent human visual inspection," *AAPS PharmSciTech*, vol. 12, no. 1, pp. 215–221, 2011.

[29] J. Z. Z. Knapp, "The scientific basis for visible particle inspection," *PDA J. Pharm. Sci. Technol.*, vol. 53, no. 6, pp. 291–302, 1999.

[30] J. Z. Knapp and H. K. Kushner, "Generalized methodology for evaluation of parenteral inspection procedures," *J. Parenter. Drug Assoc.*, vol. 34, no. 1, pp. 14–61, 1980.

Ji Ge received the B.S. and M.S. degrees in mechatronics engineering from the Jiangxi University of Science and Technology, Ganzhou, China, in 2002 and 2005, respectively, and the Ph.D. degree in pattern recognition and intelligent system from Hunan University, Changsha, China, in 2012.

He is currently a Postdoctoral Fellow with the Department of Mechanical and Industrial Engineering, University of Toronto, Toronto, ON, Canada. His research interests include machine learning, computer vision, and nanomanipulation under electron microscopy.

Shaorong Xie received the Ph.D. degree in mechanical engineering from Tianjin University, Tianjin, China, in 2001, and did her postdoctoral research in the Department of Mechanical and Industrial Engineering, University of Toronto, Toronto, ON, Canada.

She is currently a Professor with the School of Mechatronic Engineering and Automation, Shanghai University, Shanghai, China.

Prof. Xie was the recipient of the Excellent Subject Chief Scientist of Shanghai Municipality in 2012, Rising-Star of Science and Technology of Shanghai Municipality, in 2012 and 2007, the research project, "The system of underwater detection and removing risks based on special robots," won the 2011 First-Place Technological Invention Award of Shanghai Municipality (1st Awardee), and the ShuGuang Scholar of Shanghai Municipal Education Commission in 2009.

Yaonan Wang received the B.S. degree in computer engineering from East China Institute of Technology, Fuzhou, Jiangxi, China, in 1981, and the M.S. and Ph.D. degrees in control engineering from Hunan University, Changsha, China, in 1990 and 1994, respectively.

He is currently a Professor with the College of Electrical and Information Engineering, Hunan University. His research interests include machine vision, special robots, and intelligent control.

Jun Liu received the B.E. degree in automation and the B.S. degree in economics from Shandong University, Jinan, Shandong, China, in 2008. He is currently working towards the Ph.D. degree at the Advanced Micro and Nanosystems Laboratory, University of Toronto, Toronto, ON, Canada.

His research focuses on micro/nano robotics, and particularly automated manipulation of biomaterials. He is also interested in applications of computer vision algorithms, and development of new micro/nano technology for single cell biology.

Hui Zhang received the B.S., M.S., and Ph.D. degrees in pattern recognition and intelligent system from Hunan University, Changsha, China, in 2004, 2007, and 2012, respectively.

He is currently an Assistant Professor with the College of Electrical and Information Engineering, Changsha University of Science and Technology, Changsha, China. His research interests include machine vision and visual detection.

Bowen Zhou received the Ph.D. degree from the College of Electrical and Information Engineering, Hunan University, Changsha, China, in 2012.

He was a Postdoctoral Fellow with the Department of Electrical Engineering, Tsinghua University, Beijing, China. Now, he is a Lecturer with the Department of Electrical Engineering, Hunan University of Science and Technology, Xiangtan, China. His research interests include the applications of image processing and recognition in image/video matting, registration and industrial inspection.

Falu Weng received the B.S. and M.S. degrees in mechatronics engineering from Jiangxi University of Science and Technology, Ganzhou, China, in 2002 and 2005, respectively, and the Ph.D. degree in control science and engineering at Zhejiang University, Hangzhou, China, in 2013.

He is currently an Associate Professor with the College of Electrical Engineering and Automation, Jiangxi University of Science and Technology. His research interests include robust control, structural system control, time-delay systems and applications.

Changhai Ru received the B.S. and M.S. degrees in mechanical engineering from Harbin University of Commerce, Harbin, China, in 1999 and 2002, respectively, and the Ph.D. degree in mechanical engineering from the Harbin Institute of Technology, Harbin, China, in 2005.

He is a Professor with the Research Center of Robotics and Micro System, Soochow University, Suzhou, China. His research areas include microrobotics and nanorobotic manipulation, nanopositioning technology, and automated instrumentation for biomedical applications.

Chao Zhou received the B.S. degree (Hons.) in automation from Southeast University, Nanjing, China, in 2003, and the Ph.D. degree in control theory and control engineering from the Institute of Automation, Chinese Academy of Sciences, Beijing, China, in 2008.

Since July 2008, he has been an Assistant Professor with the Key Laboratory of Complex Systems and Intelligent Science, Institute of Automation, Chinese Academy of Sciences, where he has been an Associate Professor since 2011. His current research interests include the motion control of robot, the bio-inspired robotic fish, and embedded system of robot.

Min Tan received the B.S. degrees from Tsinghua University, Beijing, China, in 1986, and the Ph.D. degree from the Institute of Automation, Chinese Academy of Sciences (IACAS), Beijing, China, in 1990, both in control theory and control engineering.

He is currently a Professor with the State Key Laboratory of Complex Systems and Intelligent Science, IACAS. He has published more than 100 papers in journals, books and conference proceedings. His research interests include robotics and intelligent control system.

Yu Sun received the Ph.D. degree in mechanical engineering from the University of Minnesota, Duluth, MN, USA, in 2003, and did his postdoctoral research at ETH-Zürich.

He is a Professor with the Department of Mechanical and Industrial Engineering, with joint appointments at the Institute of Biomaterials and Biomedical Engineering and the Department of Electrical and Computer Engineering, University of Toronto. He is presently the Canada Research Chair in Micro and Nano Engineering Systems. From 2012 to 2013, he directed the University of Toronto Nanofabrication Center.

Prof. Sun was the recipient of the McLean Award, the First Prize in Technical Achievement of the American Society for Reproductive Medicine (ASRM), and the NSERC E.W.R. Steacie Memorial Fellowship. He was elected Fellow of the American Society of Mechanical Engineers (ASME), the Institute of Electrical and Electronics Engineers, and the Canadian Academy of Engineering (CAE) for his work on micro-nano devices and robotic systems. He served and serves on the Editorial Boards of several IEEE TRANSACTIONS, the *Journal of Micromechanics Microengineering*, *Scientific Reports*, and *Microsystems & Nanoengineering*.